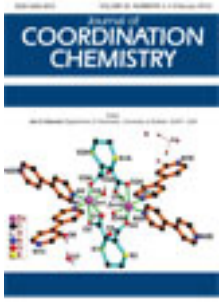

Journal of Coordination Chemistry
Publication details, including instructions for authors and subscription information:
http://www.tandfonline.com/loi/gcoo20

Transition metal complexes of 3-acetylpyridine ^{4} N-(2-pyridyl)thiosemicarbazone (HAPS); structural, spectroscopic, and biological studies

Usama El-Ayaan [a] [b]

[a] Department of Chemistry, Faculty of Science , Mansoura University , Mansoura 35516 , Egypt

[b] Department of Chemistry , College of Science, King Faisal University , P.O. Box 380, Hofuf 31982 , Saudi Arabia

Published online: 06 Feb 2012.

To cite this article: Usama El-Ayaan (2012) Transition metal complexes of 3-acetylpyridine ^{4} N-(2-pyridyl)thiosemicarbazone (HAPS); structural, spectroscopic, and biological studies, Journal of Coordination Chemistry, 65:4, 629-642, DOI: 10.1080/00958972.2012.658381

To link to this article: http://dx.doi.org/10.1080/00958972.2012.658381

Journal of Coordination Chemistry
Vol. 65, No. 4, 20 February 2012, 629–642

Transition metal complexes of 3-acetylpyridine ^4N-(2-pyridyl)thiosemicarbazone (HAPS); structural, spectroscopic, and biological studies

USAMA EL-AYAAN*†‡

†Department of Chemistry, Faculty of Science, Mansoura University, Mansoura 35516, Egypt
‡Department of Chemistry, College of Science, King Faisal University, P.O. Box 380, Hofuf 31982, Saudi Arabia

(*Received 5 September 2011; in final form 19 December 2011*)

This work examines transition metal ion complexes which have been synthesized from 3-acetylpyridine ^4N-(2-pyridyl)thiosemicarbazone (HAPS) (**1**). $[Cu(HAPS)_2Cl_2]\cdot H_2O$ (**2**), $[Hg(HAPS)_2Cl_2]$ (**3**), $[Ni(HAPS)Cl_2]\cdot 2H_2O$ (**4**), $[UO_2(APS)_2]\cdot 2H_2O$ (**5**), $[VO(HAPS)_2]SO_4\cdot H_2O$ (**6**), and $[Zn(HAPS)_2Cl_2]$ (**7**) were characterized by elemental analysis, spectral (IR, ^{1}H-NMR, and UV-Vis), magnetic, and molar conductance measurements. The biochemical studies showed that **2** and **3** have powerful and complete degradation on both DNA and protein. Complexes **2**, **4**, and **7** showed significant antioxidant properties, especially scavenging on superoxide and hydroxyl radicals. The antibacterial screening demonstrated that all studied complexes have maximum and broad range activities against Gram-positive and Gram-negative bacterial strains.

Keywords: 3-Acetylpyridine; Thiosemicarbazone complexes; Spectroscopy; Antioxidant; Antibacterial

1. Introduction

Thiosemicarbazones show a wide range of biological properties depending on the parent aldehyde or ketone; in particular, if these are heterocyclic aromatic systems, their nature enhances their activities. Thiosemicarbazones are of interest because of their chemistry and potentially beneficial biological activities, such as antitumor, antibacterial, antiviral, and antimalarial activities [1, 2]. Biological activities of thiosemicarbazones are due to their ability to form chelates with heavy metals [3, 4]. Biological activities of the metal complexes differ from those of either the ligand or the metal ion itself, and increased and/or decreased biological activities are reported for several transition metal complexes [5, 6]. The π-delocalization of charge and the configurational flexibility of the molecular chain can give a great variety of coordination modes [7]. Attachment of the thiosemicarbazone to the pyridine ring 3- or 4-position causes decrease in activity when compared to the 2-position, presumably due to a lesser ability

*Email: uelayaan@kfu.edu.sa

Journal of Coordination Chemistry
ISSN 0095-8972 print/ISSN 1029-0389 online
http://dx.doi.org/10.1080/00958972.2012.658381

to coordinate metal ions [8]. Therefore, these thiosemicarbazones have not been studied much, and N(4)-substituted thiosemicarbazones have received even less attention [9].

In this article we prepare the new ligand 3-acetylpyridine ^4N-(2-pyridyl)thiosemicarbazone (HAPS) and study its ligational behavior toward Cu^{2+}, Hg^{2+}, Ni^{2+}, UO_2^{2+}, VO^{2+}, and Zn^{2+}. Spectroscopic and magnetic moment measurements of complexes in addition to degradation effect on both DNA and protein, superoxide dismutase (SOD)-like activity, and antibacterial activities against Gram-positive and Gram-negative bacteria are discussed.

2. Experimental

2.1. *Instrumentation and materials*

All starting materials were purchased from Fluka and Aldrich and used as received. Elemental analyses (C, H, and N) were performed on a Perkin-Elmer 2400 Series II Analyzer. The molar conductivities of freshly prepared 10^{-3} mol L^{-1} dimethylformamide (DMF) solutions were measured for all studied complexes using a Mettler Toledo S70 Advanced conductivity meter. Electronic spectra were recorded on a Shimadzu UV-Vis 1800 spectrophotometer using 10 mm path length quartz cells at room temperature. Fast atom bombardment (FAB)-mass spectra were recorded on a Jeol SX 102/Da-600 mass spectrophotometer/Data system using Argon/Xenon (6 kV, 10 mA) as the FAB gas. The accelerating voltage was 10 kV and spectra were recorded at room temperature. Magnetic susceptibility was measured with a Sherwood Scientific magnetic susceptibility balance at room temperature. Infrared (IR) spectra were recorded on a Shimadzu FTIR Spectrometer 8400 as KBr pellets from 4000 to 400 cm^{-1}. ^{1}H- and ^{13}C-NMR measurements at room temperature were obtained on a Jeol JNM LA 500 WB spectrometer at 250 MHz using a 5 mm probe in $CDCl_3$.

2.2. *Preparation of 3-acetylpyridine ^{4}N-(2-pyridyl)thiosemicarbazone (HAPS)*

The ligand was prepared by boiling an ethanolic solution of 4-(2-pyridyl)-3-thiosemicarbazide (1.68 g, 10 mmol) [4] and 3-acetyl pyridine (1.21 g, 10 mmol). Yellow crystals of HAPS were removed by filtration, washed with ethanol, and recrystallized from hot ethanol, m.p. 205, yield 2.10 g (77.5%). $C_{13}H_{13}N_5S$ (271.13) Calcd: C, 57.54; H, 4.83; N, 25.81; S, 11.82. Found (%): C, 57.15; H, 4.75; N, 24.3; S, 11.56. FAB-mass spectra reveal peaks at $m/z = 271$ for the parent ligand, $C_{13}H_{13}N_5S$. Other intense peaks are also observed at m/z of 177, 93, 134, and 137 corresponding to the fragments $C_8H_7N_3S$, $C_5H_5N_2$, $C_7H_8N_3$, and $C_6H_5N_2S$, respectively.

2.3. *Synthesis of metal complexes*

All complexes were prepared by refluxing HAPS (0.7 g, 2.0 mmol) and the hydrated metal salts (1.0 mmol), e.g., chloride or acetate, in 30 mL ethanol for 2–3 h. The resulting solid complexes were filtered while hot, washed with ethanol followed by diethyl ether, and dried *in vacuo* over $CaCl_2$. All complexes are insoluble in common

organic solvents except dimethylsulfoxide (DMSO) and DMF. The molar conductivities of complexes were measured in 10^{-3} mol L^{-1} DMF solution and indicate non-electrolytes [10].

Complex **2**, $[Cu(HAPS)_2Cl_2]\cdot H_2O$, Yield (0.60 g, 86%); Anal. Calcd for $C_{26}Cl_2CuH_{28}N_{10}OS_2$: C, 44.92; H, 4.06; N, 10.07. Found (%): C, 45.21; H, 4.12; N, 10.02; *m/z*: 677.13 $[C_{26}Cl_2CuH_{26}N_{10}S_2]$. Other species are observed at *m/z* of 606 and 335, related to $[Cu(HAPS)_2]$ and [Cu(HAPS)], respectively, and finally demetallation gave fragment ion peak at *m/z* of 271.

Complex **3**, $[Hg(HAPS)_2Cl_2]$, Yield (0.72 g, 87%); Anal. Calcd for $C_{26}Cl_2H_{26}HgN_{10}S_2$: C, 38.35; H, 3.22; N, 17.20. Found (%): C, 38.21; H, 3.20; N, 17.00; *m/z*: 814.18 $[Hg(HAPS)_2Cl_2]$, 778 $[Hg(HAPS)_2Cl]$, and 743 $[Hg(HAPS)_2]$.

Complex **4**, $[Ni(HAPS)Cl_2]\cdot 2H_2O$, Yield (0.39 g, 89%); Anal. Calcd for $C_{13}Cl_2H_{17}N_5NiO_2S$: C, 35.73; H, 3.92; N, 16.03. Found (%): C, 35.51; H, 3.85; N, 15.85; the FAB-mass spectrum shows a molecular ion (M^+) peak at *m/z*: 400.94 for $[Ni(HAPS)Cl_2]$, which suggests the monomeric nature of the complex and confirm the proposed formula.

Complex **5**, $[UO_2(APS)_2]\cdot 2H_2O$, Yield (0.75 g, 88%); Anal. Calcd for $C_{26}H_{28}N_{10}O_4S_2U$: C, 36.88; H, 3.33; N, 16.54. Found (%): C, 36.55; H, 3.15; N, 16.25; *m/z*: 810.69 $[C_{26}H_{24}N_{10}O_2S_2U]$.

Complex **6**, $[VO(HAPS)_2]SO_4\cdot H_2O$, Yield (0.59 g, 82%); Anal. Calcd for $C_{26}H_{28}N_{10}O_6S_3V$: C, 43.15; H, 3.90; N, 19.35. Found (%): C, 43.10; H, 3.85; N, 19.00; *m/z*: 705.68 $[VO(HAPS)_2]SO_4$; other intense peaks are observed at 609 and 338 related to $[VO(HAPS)_2]$ and [VO(HAPS)], respectively.

Complex **7**, $[Zn(HAPS)_2Cl_2]$, Yield (0.53 g, 77%); Anal. Calcd for $C_{26}Cl_2H_{26}N_{10}S_2Zn$: C, 45.99; H, 3.86; N, 20.63. Found (%): C, 45.87; H, 3.74; N, 20.50; *m/z*: 678.9 $[Zn(HAPS)_2Cl_2]$, 643$[Zn(HAPS)_2Cl]$, 608 $[Zn(HAPS)_2]$, and 337 [Zn(HAPS)].

2.4. *Molecular modeling*

An attempt to gain a better insight on the molecular structure of HAPS and its complexes, geometry optimization, and conformational analysis has been performed by the use of MM+ [11] forcefield as implemented in Hyperchem 7.5 [12].

2.5. *Biological studies*

2.5.1. DNA agarose gel electrophoreses. HAPS or its Cu(II), Hg(II), Ni(II), UO_2(II), VO(II), and Zn(II) complexes (10 μmol L^{-1}) were added individually to 1 μg of DNA purified from *Escherichia coli* strain W3110 as described by Genthner *et al.* [13]. The samples were incubated for 1 h at 37°C. The DNA was analyzed by using horizontal agarose gel electrophoresis. The electrophoresis was carried out by utilizing 0.8% (w/v) agarose gel in TBE buffer (10 mmol L^{-1} boric acid, 1 mmol L^{-1} EDTA, and 0.04 mol L^{-1} Tris-HCl pH 7.9). The agarose gel was stained with ethidium bromide (0.5 μg mL^{-1}) and the DNA was visualized on a UV transilluminator [14].

2.5.2. Protein gel electrophoresis. Egg albumin (5 μg) was treated with HAPS or its Cu(II), Hg(II), Ni(II), UO_2(II), VO(II), and Zn(II) complexes (10 μmol L^{-1}) individually. The reaction mixtures were incubated for 1 h at 37°C. The protein samples were analyzed by using vertical 1-D SDS-polyacrylamide gel electrophoresis according to the method of Laemmli [15].

2.5.3. Scavenging activities of superoxide radicals. Scavenging activity of superoxide radicals was determined according to the method described by Liu and Ng [16]. Superoxide radicals were generated in a phenazine methosulfate (PMS), nicotinamide adenine dinucleotide (NADH) system by oxidation of NADH, and were assayed by reduction of nitroblue tetrazolium (NBT). The superoxide radicals were generated in 2 mL of 16 mmol L^{-1} Tris-HCl buffer (pH 8.0), which contained 78 μmol L^{-1} NADH, 50 μmol L^{-1} NBT, 10 μmol L^{-1} PMS, and HAPS or its metal complexes (10 μmol L^{-1}). The reaction between superoxide radicals and NBT was detected at 560 nm. *l*-Ascorbic acid at 10 μmol L^{-1} was used as a positive control. The reactions in control and samples in the presence of complexes were measured for 4 min.

The superoxide radical scavenging ratio (%) was calculated using the formula: superoxide radical scavenging ratio $(\%) = (\Delta A - \Delta A_1/\Delta A) \times 100$, where A is the absorbance of positive control and A_1 is the absorbance of the test samples.

2.5.4. Scavenging activities of hydroxyl radicals. Scavenging activity of hydroxyl radicals was carried out as described by Kang *et al.* [17]. Hydroxyl radicals were generated in an *l*-ascorbic acid-$CuSO_4$ system by reduction of Cu^{2+} and were assayed by oxidation of cytochrome *c*. The hydroxyl radicals were generated in 2 mL of 10 mmol L^{-1} sodium phosphate buffer (pH 7.4) containing 100 μmol L^{-1} ascorbic acid, 100 μmol L^{-1} $CuSO_4$, 12 μmol L^{-1} cytochrome *c*, and the tested ligand or its metal complexes (10 μmol L^{-1}). The change in absorbance caused by the oxidation of cytochrome *c* was measured at 550 nm. Thiourea was used as a positive control.

The scavenging activity of hydroxyl radical was calculated using the formula: hydroxyl radical scavenging activity $(\%) = (A - A_0/A_T - A_0) \times 100$, where A is the absorbance of samples, and A_T and A_0 are the absorbance of the thiourea and the control, respectively.

2.5.5. Antimicrobial activity. The antimicrobial test of HAPS and its metal complexes was determined using cup diffusion technique according to the method described by Bauer *et al.* [18]. The test was done against the Gram-negative bacterial strains *Pseudomonas aeruginosa*, *E. coli*, and *Erwinia carotovora*, the Gram-positive bacterial strains *Bacillus thuringiensis* and *Staphylococcus pasteuri*, and the yeast as a fungus. The tested free HAPS or its metal complexes were dissolved in DMSO at 1 mg mL^{-1}. The Luria-Bertani agar (LBA) medium (10 g bacto-tryptone, 5 g yeast extract, 10 g NaCl, and 20 g agar in 1 L de-ionized water) was made for inoculation and bacterial growth. An aliquot of the solution of the parent ligand and the tested complexes equivalent to 100 μg was placed separately in cups cut in the agar plate. The LBA plates were incubated for 24 h at 37°C and the resulting inhibition zones were measured. DMSO, which exhibited no antimicrobial activity, was used as negative control and ampicillin

Table 1. Analytical and physical data of HAPS and its metal complexes.

Compound, Empirical formula	(F. Wt)	Color	%Calcd (Found) C	H	N
(HAPS), $C_{13}H_{13}N_5S$	(271.34)	White	57.54 (57.32)	4.83 (4.30)	25.81 (24.50)
$[Cu(HAPS)_2Cl_2]\cdot H_2O$, $C_{26}Cl_2CuH_{28}N_{10}OS_2$	(695.15)	Blue	44.92 (45.21)	4.06 (4.12)	10.07 (10.02)
$[Hg(HAPS)_2Cl_2]$, $C_{26}Cl_2H_{26}HgN_{10}S_2$	(814.18)	Grey	38.35 (38.21)	3.22 (3.20)	17.20 (17.00)
$[Ni(HAPS)Cl_2]\cdot 2H_2O$, $C_{13}Cl_2H_{17}N_5NiO_2S$	(436.97)	Yellowish-orange	35.73 (35.51)	3.92 (3.85)	16.03 (15.85)
$[UO_2(APS)_2]\cdot 2H_2O$, $C_{26}H_{28}N_{10}O_4S_2U$	(846.72)	Yellow	36.88 (36.55)	3.33 (3.15)	16.54 (16.25)
$[VO(HAPS)_2]SO_4\cdot H_2O$, $C_{26}H_{28}N_{10}O_6S_3V$	(723.7)	Olive green	43.15 (43.10)	3.90 (3.85)	19.35 (19.00)
$[Zn(HAPS)_2Cl_2]$, $C_{26}Cl_2H_{26}N_{10}S_2Zn$	(678.98)	Yellow	45.99 (45.87)	3.86 (3.74)	20.63 (20.50)

(100 μg) was utilized as a positive control. From the inhibition zone diameter data, the antimicrobial activity against the Gram-negative, Gram-positive bacterial strains and yeast were determined.

3. Results and discussion

Analytical and physical data of HAPS and its metal complexes are presented in table 1.

3.1. *IR and NMR spectra of free HAPS*

^{1}H-NMR studies in DMSO-d_6 showed three tautomers (*E*-, *E′*-, and *E″*-forms) present in solution (figure 1) [19]. Proton resonance of both (^{2}NH and ^{4}NH) groups at $\delta = 5.21$ ppm for the *E*-form were observed. A low-field signal at $\delta = 14.96$ ppm assignable to (S–H $\cdots$ N) is observed for the hydrogen-bonded *E′*-isomer, with the ^{4}NH found at $\delta = 10.55$ ppm. For the third isomer, *E″* proton resonance of SH is observed at $\delta = 12.56$ ppm with ^{4}NH found at $\delta = 11.08$ ppm. Additional spectroscopic evidence about the presence of these isomers [20, 21] is indicated by the two peaks resonating at $\delta = 2.40$ and 2.47 ppm assignable to the ^{7}C*Me* hydrogen atoms. Two peaks due to pyridyl ring proton $^{4'}$CH ($\delta = 8.57$ and 8.12 ppm) and two other peaks due to pyridyl ring proton $^{3''}$CH ($\delta = 7.08$ and 7.09 ppm) were also observed [22]. Geometry optimization and conformational analysis have been applied to the ligand for all possible structural isomers and the three isomers have been confirmed.

IR spectra of HAPS (in KBr) show two bands at 1607 and 1575 cm^{-1} which are assigned to $\nu_{C=N}$ (azomethine) and $[\nu_{C=C} + \nu_{C=N}]$ of the pyridyl ring, respectively. Bands at 3165 and 3222 cm^{-1} are assigned to ν^2_{NH} and ν^4_{NH}, respectively. The possibility of thione/thiol tautomerism (HN−C=S/N=C−SH) is suggested because of the band observed at 2326 cm^{-1}. Three bands are observed at 837, 470, and 1028 cm^{-1}, corresponding to ν(CS), ν(NCS), and ν(NN), respectively. Coordination of the pyridyl nitrogen to the central metal can be followed by observing the two ring deformation bands at 610 and 407 cm^{-1} for one pyridyl nitrogen and at 630 and 427 cm^{-1} for the other.

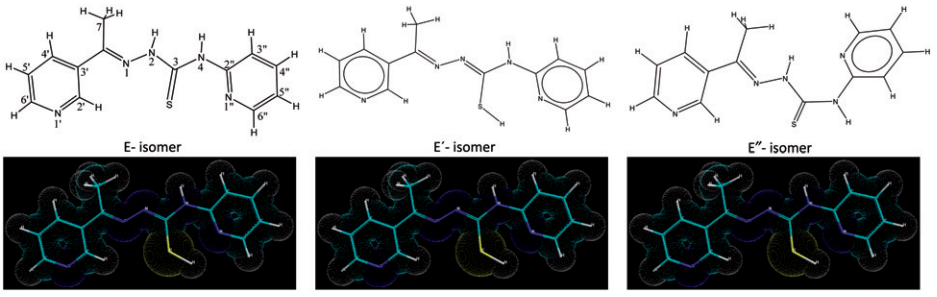

Figure 1. Structural isomers (E, E',E'') of HAPS.

Table 2. Assignments of the IR spectral bands (cm^{-1}) of HAPS and its complexes.

Compound	υ^{2}_{NH}	υ^{4}_{NH}	ν_{OH}	ν_{SH}	$\nu_{C=N}$	$\nu_{C=S}$	ν_{C-S}	ν_{M-N}	ν_{M-S}
(HAPS), **1**	3165	3222	–	2362	1607	837	636	–	–
$[Cu(HAPS)_2Cl_2]\cdot H_2O$, **2**	3072	3336	3448	–	1618 1595	808	–	515	499
$[Hg(HAPS)_2Cl_2]$, **3**	3049	3148	3492	–	1641 1608	815	–	520	480
$[Ni(HAPS)Cl_2]\cdot 2H_2O$, **4**	3065	3200	3450	–	1608	820	–	519	424
$[UO_2(APS)_2]\cdot 2H_2O$, **5**	*	*	3450	–	1653 1607	–	694	540	440
$[VO(HAPS)_2]SO_4\cdot H_2O$, **6**	3100	3200	3500	2073	1653 1624	820	–	515	472
$[Zn(HAPS)_2Cl_2]$, **7**	3186	3228	–	–	1647 1610	823	–	520	440

*A broad band due to water molecule prohibits the detection of NH bands due to **5**.

3.2. *IR and NMR spectra of complexes*

Important IR bands for the free ligand and complexes with their tentative assignments are presented in table 2.

In all complexes, coordination of either pyridyl nitrogen to the central metal is ruled out, because the positions of the bands assigned to ring deformation in the free HAPS remain unchanged in complexes.

In **2**, **3**, and **7** (figure 2), HAPS is a neutral bidentate ligand coordinating *via* azomethine nitrogen and thione sulfur. This behavior is revealed by: (i) the ν(C=N) vibration is observed at 1607 cm^{-1} for HAPS and at 1618, 1595 cm^{-1} for **2**, 1641, 1608 cm^{-1} for **3**, and at 1647, 1610 cm^{-1} for **7**, (ii) the clear change in both intensity and position of the thioamide IV bands. ^{1}H-NMR spectra of **3** and **7** show signals at 2.46 ppm in both complexes with integration equivalent to six protons assigned to two methyl groups, indicating coordination of two ligands in these complexes. In **3**, two peaks are observed at 11.49 and 11.60 ppm assignable to ^{4}NH and ^{2}NH, respectively. In **7**, these bands are observed at 9.0 and 11.1 ppm. The absence of signals due to SH (observed at 14.96 ppm in free HAPS) in the complexes is further evidence for the neutral bidentate ligand.

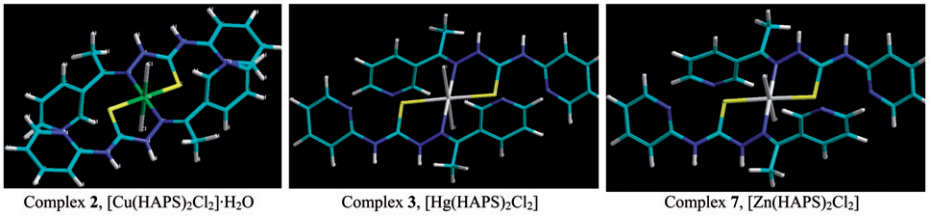

Figure 2. Structures of **2**, **3** and **7**.

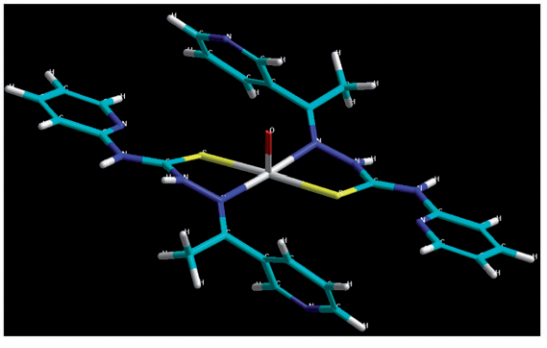

Figure 3. Structure of **6**, $[VO(HAPS)_2]SO_4 \cdot H_2O$.

A new band at 970 cm^{-1} in the spectrum of the vanadyl complex (figure 3), not observed in the free ligand, is assigned to V=O asymmetric stretching frequency.

The coordination sphere of the uranyl(VI) centre contains the oxo ligands in apical positions with a planar equatorial coordination environment containing two bidentate N,S-ligands (figure 4). This was confirmed as follows: the ligand is binegative, coordinating *via* thiol sulfur confirmed by the disappearance of both ^{4}NH and ^{2}NH in the ^{1}H-NMR spectra of **6**. The uranyl complex exhibits three bands at 918, 810, and 270 cm^{-1} assigned to ν_3, ν_1, and ν_4 vibrations, respectively, of the dioxouranium [23, 24]. The force constant (F) for ν(U=O) is calculated by the method of McGlynn *et al.* [25].

$$(\nu_3)^2 = (1307)^2(F_{U-O})/14.1$$

The F_{U-O} is 6.96 m dynes $Å^{-1}$; the U–O bond distance is calculated as [26]:

$$R_{U-O} = 1.08F^{-1/3} + 1017.$$

The U–O bond distance (1.74 Å) falls in the usual region [27].

3.3. *Electronic spectra and magnetic moment of complexes*

Electronic spectra were measured in 10^{-3} mol L^{-1} DMSO solution for all complexes. Tentative assignments of the significant electronic spectral absorption bands of HAPS

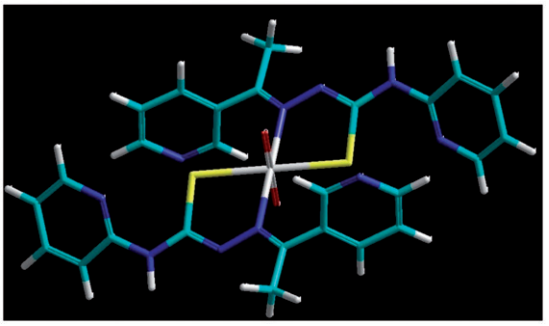

Figure 4. Structure of **5**, $[UO_2(APS)_2]\cdot 2H_2O$.

Table 3. Magnetic moments (B.M.) and electronic spectral bands (cm^{-1}) of the complexes.

Complex	μ_{eff} (B.M.)	d–d transition (cm^{-1})	Intraligand and charge transfer (cm^{-1})
$[Cu(HAPS)_2Cl_2]\cdot H_2O$, **2**	2.10	16,778 (0.75)	32,258; 27,933; and 22,831
$[Ni(HAPS)Cl_2]\cdot 2H_2O$, **4**	3.57	22,936 (0.57)	33,113 and 29,412
$[UO_2(APS)_2]\cdot 2H_2O$, **5**	diamagnetic	–	33,496; 31,722; 27,612; and 21,910
$[VO(HAPS)_2]SO_4\cdot H_2O$, **6**	1.724	12,285 (0.38)	35,461; 27,933; and 25,641
$[Zn(HAPS)_2Cl_2]$, **7**	diamagnetic	–	33,113; 31,446; 27,624; and 21,930

Values of ε_{max} are in parentheses and multiplied by 10^{-4} $((mol\ L^{-1})^{-1}cm^{-1})$.

and its metal complexes are given in table 3. In all complexes three maxima are observed at 27,900–29,400, 32,260–33,110, and 35,200–36,500 cm^{-1} associated with $n\rightarrow\pi^*$ transition of the thiosemicarbazone.

Magnetic moment measurements of $[Cu(HAPS)_2Cl_2]\cdot H_2O$ (**2**) of 2.1 B.M. correspond to one unpaired electron. Electronic spectra of **2** show one low intensity band at 16,778 cm^{-1} assigned to $^2B_{1g}\rightarrow{}^2B_{2g}$ ($d_{x2-y2}\rightarrow d_{zy}$) transition and two strong bands at 22,831 and 27,933 cm^{-1} are assigned to $^2B\rightarrow{}^2E_g$ and ligand-to-metal charge transfer (LMCT) transitions, respectively. These transitions suggest octahedral [28].

$^3T_1(F)\rightarrow{}^3T_1(P)$ transition in $[Ni(HAPS)Cl_2]\cdot 2H_2O$ (**4**) (figure 5) appears as a low intensity band at 19,530 cm^{-1}. In addition, two strong bands are also observed at 22,936 and 29,412 cm^{-1}, assigned to LMCT bands and $\pi\rightarrow\pi^*$ transitions, respectively. Magnetic moment of 3.57 B.M. is additional evidence for tetrahedral geometry around Ni(II) [29].

The electronic spectra of $[UO_2(APS)_2]\cdot 2H_2O$ (**5**) exhibit several bands in the range of 50,000–14,000 cm^{-1}. Bands at 33,000–30,000 cm^{-1} coincide with bands observed in the free ligand. Some of these bands are slightly shifted to lower energy compared to the free ligand transitions because of coordination with the U(VI). Since these are intraligand transitions they are allowed and occur with high intensity. Two relatively less intense bands at 21,910 and 27,000 cm^{-1} can be assigned to uranyl oxygen to uranium and nitrogen to uranium charge transfer transitions, respectively [30].

In $[VO(HAPS)_2]SO_4\cdot H_2O$ (**6**), the d–d bands at 25,000 and 12,300 cm^{-1} may be attributed to $b_2(d_{xy}, d_{xz})\rightarrow a_1^*(d_{xy})$ and $b_2(d_{x2-y2})\rightarrow e_{\pi^*}(d_{xz}, d_{yz})$ transitions, respectively. The obtained electronic spectrum indicates a structure with five-coordinate,

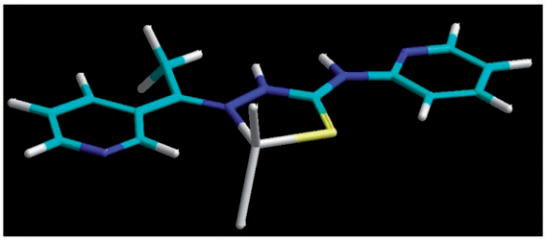

Figure 5. Structure of **4**, $[Ni(HAPS)Cl_2] \cdot 2H_2O$.

Table 4. ESR data of $[VO(HAPS)_2]SO_4 \cdot H_2O$ at room temperature.

Complex	$g_{\|\|}$	$g_\perp$	g_{iso}	G	$A_{\|\|} \times 10^{-4}$ (cm^{-1})	$A_\perp$	A_{iso}	α^2	β^2	K
$[VO(HAPS)_2]SO_4 \cdot H_2O$	1.93	1.97	1.96	2.24	165	55	91.6	0.76	0.98	0.71

probably square-pyramidal geometry [31]. The 1.724 B.M. value of magnetic susceptibility at room temperature confirms V(IV), consistent with the square-pyramidal geometry around the central vanadyl ion [32].

Electronic spectra of Zn(II) complex **7** show intense absorptions in the UV-region (21,930, 27,624, 31,446, and 33,113 cm^{-1}) which are assigned to charge transfer (LMCT) and intraligand transitions [33].

3.4. *ESR spectroscopy*

The ESR spectrum of $[VO(HAPS)_2]SO_4 \cdot H_2O$ at room temperature is shown in "Supplementary material" (figure S1). The ESR spectral data are presented in table 4. The RT spectrum is a typical eight line pattern which shows that a single vanadium is present, one set due to parallel feature and the other set due to perpendicular feature, which indicates axially symmetric anisotropy with well-resolved 16-line hyperfine splitting, characteristic of interaction between the electron and vanadium nuclear spins. The $g_{||}$ and $g_\perp$ values were computed from the spectrum. The observed $g_{||}$, $g_\perp$, $|g|$, $A_{||}$, $A_\perp$, and $|A|$ values indicate that the unpaired electron is localized in d_{xy} orbital in square-pyramidal geometry [34–36]. If $G < 4.0$, the ligand forming the complex is regarded as a strong field ligand. The G value of the complex at room temperature is 2.24, indicating that the Schiff-base ligand is a strong field ligand and the metal–ligand bonding in this complex is covalent. The molecular orbital coefficients α^2 and β^2 for $[VO(HAPS)_2]SO_4 \cdot H_2O$ complex were calculated [37–39]. Neglecting the second-order effects and taking the negative values for $A_{||}$ and $A_\perp$ and solving the last equations to obtain α^2 and β^2, where the free dipolar interaction constant "P" between magnetic moment of the electron and vanadium nucleus $= 128 \times 10^{-4}$ cm^{-1}, $g_e = 2.0023$, $A_{||}$, $A_\perp$, and $|A|$ are taken to be negative, P is the free ion dipole term $= 128 \times 10^{-4}$ cm^{-1}, λ = spin–orbit coupling constant = 170 cm^{-1}, E = electronic transition energy.

The spin–orbit coupling coefficient, λ, is assumed to be 170 cm^{-1} for VO^{2+} ion and E is the electronic transition energy of $^2B_2 \rightarrow {}^2E$ and k is the Fermi contact term which is

directly related to the isotropic hyperfine coupling and represents the amount of unpaired electron density at the nucleus.

The value of the in-plane σ-bonding coefficient α^2 generally follows the σ donor strength of the ligand, i.e., α^2 decreases as covalent bonding increases. The dependences of K on α^2 arise from participation of the empty 4s orbital on the metal in σ-bonding to the ligands. The empty 4s orbital of the metal can overlap with the filled σ-levels of the basal ligands as effectively as can the d_{x2-y2} orbital of the metal. The molecular orbital formed from the 4s orbital should put partial 4s density in a filled bonding orbital, which in turn should undergo spin polarization by the d_{xy} electron. The extent of the ligand to metal interaction should be related to both energy of antibonding d_{x2-y2} energy level and its orbital coefficient.

The 4s contribution to K should be proportional to the metal electron density in the filled orbital that contains contribution of the 4s orbital. The delocalization in the σ-system of the complex is expressed by the bonding coefficient for the d_{x2-y2} level. The origin of the isotropic constant term K, which is related to the amount of unpaired electron density on the vanadium nucleus, has been the subject of discussion. Since the orbital that contains the unpaired electron, d_{xy}, has zero electron density at the vanadium nucleus and does not mix with the metal 4s orbital (in C_{4V} symmetry), there is no direct way of putting unpaired electron density on the nucleus. The nonzero value of K must then arise from an indirect mechanism. McGravey [40] suggests that variation can be explained by involving a spin polarization mechanism. The unpaired electron in the d_{xy} orbital formally creates unpaired electron density in filled 2s and 3s orbitals of the vanadium. In the absence of covalent bonding and 4s mixing, spin polarization should remain constant and equal to the free ion value, K_O. Taking into account covalent bonding, K shows dependence on the d-orbital population for the unpaired electron, $K \sim \alpha^2 K_O$.

The lower values of α^2 compared to β^2 indicate that the in-plane σ-bonding is more covalent. These data are consistent with other reported data [41–43].

3.5. *Biochemical effect of HAPS ligand and its metal-complexes on the DNA in vitro*

Degradation of 10 μmol L^{-1} HAPS or its metal complexes on DNA *in vitro* is shown in "Supplementary material" (figure S2). Both the negative control (only DNA) and the positive control (DNA in DMSO) do not exhibit any degradation through the incubation period as represented in "Supplementary material," figure S2 lanes 1 and 2, respectively.

The ligand exhibits a weak degradation effect appearing as a smear in the area leading the DNA as shown in "Supplementary material" (figure S2 lane 3). Complex **6** degrades the DNA more than **7** as shown in "Supplementary material," figure S2 lanes 7 and 5, respectively. However, **5** arrests the DNA in the well preventing the DNA from migrating as represented in "Supplementary material" (figure S2 lane 9).

Complexes **2**, **3**, and **4** (10 μmol L^{-1}) have powerful and complete degradation on *E. coli* DNA as illustrated in "Supplementary material," figure S2 lanes 8, 4, and 6, respectively. Therefore, these complexes can be viewed as promising antitumor agents *in vivo* to arrest DNA replication in the tumor cells and not allow the tumor further growth.

Table 5. Effect of HAPS and its metal complexes on superoxide radicals generated by PMS/NADH.

Sample	Δ through 4 min	% Inhibition
Control	0.642	–
l-Ascorbic	0.098	81.9
1	0.276	57.0
2	0.185	71.2
3	0.431	32.9
4	0.207	67.8
5	0.408	36.5
6	0.393	38.8
7	0.169	73.7

To define the role of the degradation effect of free HAPS or its metal complexes on tumor cells, further biochemical studies were carried out on egg albumin as protein molecule. The effect of 10 μmol L^{-1} of the tested ligand or its metal complexes on egg albumin *in vitro* is illustrated in "Supplementary material" (figure S3). The negative control (only egg albumin) and positive control (egg albumin in DMSO) do not show any digestion effect through the incubation period as represented in "Supplementary material," figure S3 lanes 1 and 2, respectively.

HAPS has a weak digestion effect on egg albumin as illustrated in "Supplementary material," figure S3 lane 3, while **2**, **3**, **5**, and **7** have considerable digestion effect on the egg albumin as represented in "Supplementary material," figure S3 lanes 8, 4, 9, and 5, respectively. The order of digestion has the order **5** > **2** > **3** > **7**. Complexes **4** and **6** degrade completely the egg albumin as illustrated in "Supplementary material," figure S3 lanes 6 and 7, respectively.

HAPS has a weak effect on both DNA and protein. However, **7** has a considerable degradation on both DNA and egg albumin. While **2** and **3** degrade the DNA completely, less effect was observed with the egg albumin. Therefore, **2** and **3** are promising materials to arrest DNA of the tumor cells from further replication.

HAPS and its metal complexes were screened for superoxide-scavenging activity in the PMS/NADH–NBT system, and the results are presented in table 5. In this system, superoxide anion derived from dissolved oxygen by PMS/NADH coupling reduces NBT. The decrease of absorbance at 560 nm with antioxidant activities of the complexes indicates the consumption of superoxide anion in the reaction mixture. There was a difference in the overall scavenging ability among HAPS and its metal complexes. HAPS, **2**, **4**, and **7** display scavenging activities greater than 50% of the superoxide radical, as represented in table 5, while **3**, **5**, and **6** exhibit scavenging activity lower than 50%, as illustrated in table 5. Among the complexes, **7** shows the highest scavenging activity of superoxide radical in this system. Superoxide is a major factor in radiation damage, inflammation, and tumor promotion. Fortunately, this study has evolved a defense system against the toxicity of O_2^- by **2**, **4**, and **7**.

The subcellular compartmentation of defense mechanisms is essential for efficient removal of O_2^- and H_2O_2 at sites where they are generated throughout the cell [44]. It is significant to find SOD mimics, which have the activity of SOD and at the same time are stable. Dismutation of superoxide forms hydrogen peroxide and in the presence of

Table 6. Effect of HAPS and its metal complexes on hydroxyl radicals generated by *l*-ascorbic acid/Cu^{2+} system.

Sample	OD_{550}	% Inhibition
Control	0.198	–
Thiourea	0.714	100
1	0.382	35.7
2	0.604	78.7
3	0.418	42.6
4	0.596	77.1
5	0.378	34.9
6	0.486	55.8
7	0.547	67.6

transition metals, the Fenton reaction produces hydroxyl radicals from the substrate hydrogen peroxide. There are two kinds of SOD mimics: metal-dependent and metal-independent mimics. This work focused on the metal-dependent SOD mimics, their assays, chemical character, and usage. SOD or the metal complexes catalyze the dismutation of superoxide according to the following equations:

The metal cation M^{n+} in complex is reduced to $M^{(n-1)+}$ and reoxidized back to M^{n+}

$$M^{n+} + O_2^{\bullet -} \rightarrow M^{(n-1)+} + O_2, \tag{1}$$

$$M^{(n-1)+} + O_2^{\bullet -} + 2H^+ \rightarrow M^{n+} + H_2O_2, \tag{2}$$

$$2O_2^{\bullet -} + 2H^+ \rightarrow H_2O_2 + O_2. \tag{3}$$

Table 6 shows the scavenging effect of HAPS and metal complexes on hydroxyl radicals. The hydroxyl radicals were generated in an *l*-ascorbic acid/$CuSO_4$ system and were assayed by the oxidation of cytochrome *c*. High-scavenging activity more than 50% was recorded with **2**, **4**, **6**, and **7**, as illustrated in table 6. HAPS, **3**, and **5** have scavenging activity lower than 50%, as illustrated in table 6.

HAPS and its metal complexes are water insoluble; therefore, the antimicrobial test was carried out in DMSO. The DMSO was used as a negative control and ampicillin was utilized as a positive control for the antimicrobial tests. The results of the antimicrobial tests against Gram-negative bacterial strains *P. aeruginosa*, *E. coli*, and *E. carotovora*, Gram-positive bacterial strains *B. thuringiensis* and *S. pasteuri*, and yeast as a fungus are illustrated in table 7.

The parent ligand has considerable antimicrobial activity with inhibition zone diameter against *P. aeruginosa* 15 mm, and *E. carotovora* 16 mm, the Gram-positive bacterial strains *B. thuringiensis* 18 mm and *S. pasteuri* 14 mm, the yeast 18 mm and a moderate effect against *E. coli* 8 mm (table 7). All complexes display a strong antimicrobial activity against the tested Gram-negative, Gram-positive bacterial strains, and fungus. The antimicrobial activity of the complexes is stronger than ampicillin as positive control (table 7). All complexes can be utilized as antimicrobial broad spectrum compounds against Gram-negative, Gram-positive bacterial strains, and fungus after further biological studies to elucidate its entire role *in vivo*.

Table 7. The antimicrobial effect of HAPS and its metal complexes, expressed as zone of inhibition in millimeter diameter.

Compound	*E. coli*	*P. aeruginosa*	*S. pasteuri*	*B. thuringiensis*	*E. carotovora*	*yeast*
Ampicillin	14	15	13	15	14	12
1	8	15	14	18	16	18
2	16	13	18	20	18	19
3	18	16	23	26	21	28
4	16	14	15	18	21	22
5	18	17	17	15	18	12
6	12	12	12	14	20	13
7	14	19	16	18	12	17

4. Conclusion

A new series of complexes, $[Cu(HAPS)_2Cl_2]\cdot H_2O$ (**2**), $[Hg(HAPS)_2Cl_2]$ (**3**), $[Ni(HAPS)Cl_2]\cdot 2H_2O$ (**4**), $[UO_2(APS)_2]\cdot 2H_2O$ (**5**), $[VO(HAPS)_2]SO_4\cdot H_2O$ (**6**), and $[Zn(HAPS)_2Cl_2]$ (**7**), were prepared from 3-acetylpyridine ^4N-(2-pyridyl)thiosemicarbazone (HAPS). Geometry optimization and conformational analysis have been performed and perfect agreement with spectral studies suggests the exact structures of the free ligand and complexes.

Biochemical studies show that **2** and **3** have powerful degradation on DNA. Compounds binding through intercalation to DNA prevent further replication, leading to death of the cell; the same mechanism is anticipated for anticancer activity of the compounds [45]. Therefore, these complexes can be used as promising antitumor agents *in vivo* to inhibit DNA replication in tumor cells. Complexes **2**, **4**, and **7** exhibit significant inhibition to superoxide radical formation and scavenging abilities on hydroxyl radicals. The antibacterial screening demonstrates that the complexes have higher antimicrobial activities than the free ligand [46] due to coordination to the metal [47]. Therefore, these complexes can be utilized as broad range spectrum compounds against Gram-positive and Gram-negative bacterial strains and fungus after further biological studies.

Attachments of the thiosemicarbazone moiety to the pyridine ring 3-position (this work) causes a decrease in activity when compared to the 2-position [4], presumably due to a lesser ability to coordinate metal ions [48].

Acknowledgments

The financial support by the Deanship of Scientific Research (Project Number 110013) King Faisal University, Saudi Arabia, is gratefully acknowledged. The author thanks Dr Magdy Youssef for helping with the biological part.

References

[1] M.X. Li, C.L. Chen, D. Zhang, J.Y. Niu, B.S. Ji. *Eur. J. Med. Chem.*, **45**, 2987 (2010).
[2] A.P. da Silva, M.V. Martini, C.M.A. de Oliveira, S. Cunha, J.E. de Carvalho, A.L.T.G. Ruiz, C.C. da Silva. *Eur. J. Med. Chem.*, **45**, 3169 (2010).

[3] G.A. El-Reash, U. El-Ayaan, I.M. Gabr, E. El-Rachawy. *J. Mol. Struct*., **969**, 33 (2010).
[4] U. El-Ayaan, M.M. Youseef, S. Al-Shihry. *J. Mol. Struct*., **936**, 213 (2009).
[5] D.X. West, S.B. Padhye, P.B. Sonawane. *Struct. Bond*., **76**, 1 (1991).
[6] A.E. Liberta, D.X. West. *BioMetals*, **5**, 121 (1992).
[7] D. Kovala-Demertzi, U. Gangadharmath, M.A. Demertzis, Y. Sanakis. *Inorg. Chem. Commun*., **8**, 619 (2005).
[8] J.P. Scovill, D. Klayman, C. Lambros, G.E. Childs, J.D. Notsch. *J. Med. Chem*., **27**, 87 (1984).
[9] H. Beraldo, R. Lima, L.R. Teixeira, A.A. Moura, D.X. West. *J. Mol. Struct*., **553**, 43 (2000).
[10] W.J. Geary. *Coord. Chem. Rev*., **7**, 81 (1971).
[11] N.L. Allinger. *J. Am. Chem. Soc*., **99**, 8127 (1977).
[12] *HyperChem Professional 7.5*, Hypercube, Inc., Gainesville, FL, USA (2002). Available online at: http://www.hyper.com (accessed 10 May 2011).
[13] F.J. Genthner, L.A Hook, W.R. Strohl. *Appl. Environ. Microbiol*., **50**, 1007 (1985).
[14] J. Sambrook, E.F. Fritsch, T. Maniatis. *Molecular Cloning: A Laboratory Manual*, Cold Spring Harbor Laboratory Press, Cold Spring Harbor, NY (1989).
[15] U.K. Laemmli. *Nature*, **689**, 227 (1970).
[16] F. Liu, T.B. Ng. *Life Sci*., **66**, 725 (2000).
[17] D.G. Kang, C.K. Yun, H.S. Lee. *J. Ethmopharmacol*., **87**, 231 (2003).
[18] A.W. Bauer, W.M. Kirby, J.C. Sherris, M. Turck. *Am. J. Clin. Pathol*., **45**, 493 (1966).
[19] K. Nomiya, K. Sekino, M. Ishikawa, A. Honda, M. Yokpyama, N.C. Kasuga, H. Yokoyama, S. Nakano, K. Onodera. *J. Inorg. Biochem*., **98**, 601 (2004).
[20] D.X. West, C.S. Carlson, A.E. Liberta, J.N. Albert, C.R. Daniel. *Transition Met. Chem*., **15**, 341 (1990).
[21] D.X. West, C.S. Carlson, K.J. Bouck, A.E. Liberta. *Transition Met. Chem*., **16**, 271 (1991).
[22] D.X. West, H. Gebremedhin, T.J. Romack, A.E. Liberta. *Transition Met. Chem*., **19**, 426 (1994).
[23] F. Quilés, A. Burneau. *Vib. Spectrosc*., **18**, 61 (1998).
[24] U. El-Ayaan, G.A. El-Reach, I.M. Kenawy. *Synth. React. Inorg. Met.-Org. Chem*., **33**, 327 (2003).
[25] S.P. McGlynn, J.K. Smith, W.C. Neely. *J. Chem. Phys*., **35**, 105 (1961).
[26] L.H. Jones. *Spectrochim. Acta*, **11**, 409 (1959).
[27] U. El-Ayaan, G.A. El-Reach, P. Weinberger, W. Linert. *Synth. React. Inorg. Met.-Org. Chem*., **30**, 1759 (2000).
[28] A.B.P. Lever. *Inorganic Spectroscopy*, 2nd Edn, Elsevier, Amsterdam (1984).
[29] A.A. El-Asmy, O.A. Al-Gammal, D.A. Saad, S.E. Ghazy. *J. Mol. Struct*., **934**, 9 (2009).
[30] S.M.E. Khalil. *J. Coord. Chem*., **56**, 1013 (2003).
[31] R.L. Farmer, F.L. Urbach. *Inorg. Chem*., **13**, 587 (1974).
[32] R. Yanardag, T.B. Demirci, B. Ulkuseven, S. Bolkent, S. Tunali, S. Bolkent. *Eur. J. Med. Chem*., **44**, 818 (2009).
[33] D. Kovala-Demertzi, A. Alexandratos, A. Papageorgiou, P.N. Yadav, P. Dalezis, M.A. Demertzis. *Polyhedron*, **27**, 2731 (2008).
[34] W. Goedey. *Theory and Application of Electronic Spin Resonance*, Wiley, New York (1980).
[35] S.K. Gupta, D. Raina. *Transition Met. Chem*., **22**, 327 (1997).
[36] A. Syamal, K.S. Kale. *Ind. J. Chem*., **17A**, 518 (1979).
[37] B.T. Thaker, J. Lekhadia, A. Patel, P. Thaker. *Transition Met. Chem*., **19**, 623 (1994).
[38] E. Martell. *Coordination Chemistry*, Vol. 1, p. 217, Van Nostrand Reinhold Co., NewYork (1971).
[39] D.U. Warad, C.D. Statish, V.H. Kulkarni, C.S. Bajgur. *Ind. J. Chem*., **39A**, 415 (2000).
[40] B.R. McGravey. *J. Chem. Phys*., **41**, 3743 (1964).
[41] B.T. Thaker, R.S. Barvalia. *Spectrochim. Acta, Part A*, **74**, 1016 (2009).
[42] N.M. El-Metwally, R.M. El-Shazly, I.M. Gabr, A.A. El-Asmy. *Spectrochim. Acta, Part A*, **61**, 1113 (2005).
[43] M.A. Neelakantana, F. Rusalraj, J. Dharmaraja, S. Johnsonraja, T. Jeyakumar, M. Sankaranarayana Pillai. *Spectrochim. Acta, Part A*, **71**, 1599 (2008).
[44] K. Asada. *Annu. Rev. Plant Physiol. Plant Mol. Biol*., **50**, 601 (1999).
[45] N.V. Kulkarni, V.K. Revankar. *J. Coord. Chem*., **64**, 725 (2011).
[46] S.A. Patil, S.N. Unki, A.D. Kulkarni, V.H. Naik, U. Kamble, P.S. Badami. *J. Coord. Chem*., **64**, 323 (2011).
[47] S.A. Patil, V.H. Naik, A.D. Kulkarni, U. Kamble, G.B. Bagihalli, P.S. Badami. *J. Coord. Chem*., **63**, 688 (2010).
[48] J.P. Padhye, G.B. Kauffman. *Coord. Chem. Rev*., **27**, 87 (1984).